RSC Advances

PAPER

View Article Online
View Journal | View Issue

Cite this: *RSC Adv.*, 2017, **7**, 16174

Synthesis of thermochemically stable tetraphenyladamantane-based microporous polymers as gas storage materials†

Xiong Li,[a] Jianwei Guo,*[a] Hangbo Yue,[a] Jiawei Wang[b] and Paul D. Topham*[b]

Received 29th December 2016
Accepted 24th February 2017

DOI: 10.1039/c6ra28833b

rsc.li/rsc-advances

In view of environmental pollution control and purification of natural gases, developing ideal porous materials for small gas molecule (hydrogen, methane and carbon dioxide) capture is an important, pressing challenge. Accordingly, herein, three microporous organic polymers (**MOP-Ad**) have been synthesized by Suzuki coupling polymerization of 1,3,5,7-tetrakis(4-bromophenyl)adamantane "knots" with three phenylboronic acid-type "rods". Gas adsorption studies of the **MOP-Ad** materials demonstrated their permanent porosity and good gas storage capabilities (1.07 wt% H_2 at 77.3 K and 1.13 bar, 10.3 wt% CO_2 and 2.4 wt% CH_4 at 273.1 K and 1.13 bar), as well as moderate CO_2/CH_4 adsorption selectivity. Moreover, high thermal stability (up to 520 °C) and remarkable chemical resistance to strong acids and bases were found in these polymers, making them suitable candidates as gas storage materials in harsh chemical environments.

1. Introduction

Advanced porous organic materials could play a pivotal role in next-generation clean energy technologies to compete with established materials such as zeolites, activated carbons and porous polymeric materials in the field of gas storage/separation, heterogeneous catalysis and chemical sensors, *etc.*[1,2] In view of environmental pollution control and purification of natural gases for fuels, developing ideal porous materials for small gas molecule (hydrogen, methane and carbon dioxide) capture has been a hot topic for some time. Metal–organic frameworks (MOFs),[3] covalent–organic frameworks (COFs)[4] and microporous organic polymers (MOPs)[5] have been reported as the most promising materials for gas capture owing to their large specific surface area, controllable pore structure, low mass density and high flexibility in structural design. For instance, Hong *et al.* reported that magnesium-based metal–organic frameworks mmen-Mg_2(dobpdc), synthesized *via* solvothermal and microwave methods, displayed excellent capacity for CO_2 adsorption (169.84 mg g^{-1} at 298 K and 1 bar) in combination with CO_2 over N_2 selectivity of over 96%.[6] Yaghi and Furukawa showed that COF-102 and COF-103 materials, prepared by self-condensation reactions of tetra(4-(dihydroxy)borylphenyl)-methane and tetra(4-(dihydroxy)borylphenyl)silane, exhibited remarkable gas uptake (1200 mg g^{-1} and 1190 mg g^{-1} for CO_2 at 298 K and 55 bar),[7,8] whilst Han and co-workers designed tetraphenylethylene-based microporous organic polymers, which also gave high CO_2/CH_4 selectivity (5.4–13.4 at 273 K and 1 bar),[9] Zou *et al.* reported work on a novel charged MOF with a nitrogen-containing tetracarboxylate ligand and indium(III) ions, which exhibited significant CO_2 adsorption capacity as well as high CO_2 adsorption selectivity over N_2 (up to 106 at 273 K and 1 bar) and CH_4 (up to 25 at 273 K and 1 bar).[10] Despite promising gas absorption capabilities, these porous materials suffer from various structural instabilities under certain conditions, a limiting factor that has not yet been fully addressed. The presence of moisture and other harsh components in mixed gases lead to the degradation of most MOF materials *via* the hydrolysis of coordinate bonds.[11] Likewise, some COF materials suffer from chemical/hydrothermal instability owing to the breakage of reversibly formed bonds, such as boroxines or imines in the structure.[7] During the past decade, much attention has also focused on the functionalization of MOP materials for gas separation. For instance, Li and Wang reported a series of nitrogen-rich microporous poly(Schiff-base)s, which exhibited excellent CO_2/CH_4 selectivity (14, 273 K and 1 bar).[12] Senker *et al.* synthesized series of microporous polyimides (MOPIs), *via* polycondensation of amine and anhydride linker molecules, which showed high CO_2/CH_4 selectivity (13, 273 K and 1 bar).[13] Nevertheless, the presence of heteroatoms (such as B, N, O, S, *etc.*) in the MOP backbones, diminished their structural stability,[14–16] compared to their non-functionalized counterparts.[17,18] Therefore, it is remains essential to search for, and develop porous organic materials that can maintain physicochemical stability especially for adsorption over long periods of time or repeated uses in harsh environments.

[a]*Guangdong University of Technology, School of Chemical Engineering and Light Industry, China. E-mail: guojw@gdut.edu.cn*

[b]*Chemical Engineering & Applied Chemistry, Aston University, UK. E-mail: p.d.topham@aston.ac.uk*

† Electronic supplementary information (ESI) available. See DOI: 10.1039/c6ra28833b

Adamantane and its derivatives, a class of unique compounds with a relatively rigid three-dimensional framework and high physicochemical stability,[19,20] have been employed as suitable building blocks in the preparation of thermostable microporous polymers.[21,22] For instance, Han and co-workers[15] reported networks of hexakis(4-bromophenyl)benzene and diethynylbenzene (HPOP-2), synthesized *via* Sonogashira coupling, possessed a high Brunauer–Emmett–Teller (BET) surface area of 742 m^2 g^{-1} but degraded around 280 °C. In contrast, Chang *et al.*[18] designed and synthesized novel MOP materials in the same way and all reagents except that 1,3,5,7-tetrakis(4-iodophenyl)adamantane were used in place of hexakis(4-bromophenyl)benzene, showing a high BET surface area (up to 665 m^2 g^{-1}) and a degradation temperature around 340 °C. They attributed the enhanced thermal stability to the introduction of adamantane into the molecular structure.

Substantially building on this pioneering work, thermochemically stable MOP based on adamantane (termed **MOP-Ad-1**, **MOP-Ad-2** and **MOP-Ad-3**) with three different "rod" lengths have been successfully synthesized *via* Suzuki coupling polymerization, as reported herein. The synthesized materials possess a crosslinked network comprising solely C–C bonds, which significantly contribute to the chemical and hydrothermal stability of the resulting polymers, and this structural design could also lead to an increase in CO_2 capture capacity as well as CO_2/CH_4 adsorption selectivity.

2. Experimental

2.1 Materials

Adamantane, benzene-1,4-diboronic acid, 4,4′-dibromobiphenyl, *p*-terphenyl, tetrakis(triphenylphosphine) palladium(0), were purchased from Shanghai Macklin Biochemical Co., Ltd, Sigma Aldrich and TCI and used as received. 1,3,5,7-Tetrakis(4-bromophenyl)adamantane (**TBPA**),[20] biphenyl-4,4′-diboronic acid[22] and 4,4″-dibromo-*p*-terphenyl[23] were prepared according to the procedures described in the literature.

2.2 Synthesis of MOP-Ad networks

Synthesis of the **MOP-Ad** series is outlined in Scheme 1. For **MOP-Ad-1**, to a mixture of **TBPA** (0.30 g, 0.40 mmol, 1.0 equiv.), benzene-1,4-diboronic acid (0.15 g, 0.91 mmol) in DMF (100 ml), tetrakis(triphenylphosphine) palladium(0) (45.85 mg, 39.68 μg, 10.0 mol%) and an aqueous solution of K_2CO_3 (2.0 M, 16.0 ml) were added. The resulting mixture was degassed *via* freeze–pump–thaw cycles, purging with Ar, and stirring at 150 °C for 72 h. After cooling to room temperature, the mixture was poured into deionized water. The precipitate was collected by filtration, and washed with water to remove the inorganic salts. Further purification of the precipitate was carried out by Soxhlet extracted with water, methanol, acetone, tetrahydrofuran and chloroform (sequentially), each of for 24 h. The polymers were dried under vacuum at 200 °C for 24 h, to give an off-white powder (0.23 g, 97.7% yield). Anal. calcd for $C_{46}H_{36}$: C, 93.88; H, 6.12. Found: C, 92.54; H, 5.43.

The synthetic procedure for **MOP-Ad-2** and **MOP-Ad-3** were similar to that of **MOP-Ad-1** except that the "rod" used was 4,4″-dibromo-*p*-terphenyl for **MOP-Ad-2** and *p*-terphenyl-4,4″-diboronic acid for **MOP-Ad-3** instead of benzene-1,4-diboronic acid. Yields were 90.2% (anal. calcd for $C_{58}H_{44}$: C, 94.05; H, 5.95. Found: C, 91.87; H, 6.15 for **MOP-Ad-2**) and 65.7% (anal. calcd for $C_{70}H_{52}$: C, 94.17; H, 5.83. Found: C, 91.99; H, 6.58 for **MOP-Ad-3**) based on hypothetical 100% polycondensation.

2.3 Characterization

^1H and ^{13}C NMR spectra were recorded on a Bruker AVANCE III 400 MHz Superconducting Fourier in dimethyl sulfoxide-d_6 (DMSO-d_6) or deuterated chloroform ($CDCl_3$) and were referenced to external tetramethylsilane (TMS). Solid-state cross polarization magic angle spinning (CP/MAS) NMR spectra were recorded on a Bruker Avance III 400 NMR spectrometer. Fourier transform infrared (FTIR) spectra were obtained using a Thermo Electron Nicolet-6700 spectrometer. Target polymers were pressed into KBr pellets for the spectral measurements. Powder X-ray diffraction (XRD) data were collected on a Bruker X'pertpro multipurpose diffractometer (MPD). Samples were mounted on a sample holder and measured using Cu Kα radiation with a 2θ range of 5° to 80°. Small-angle X-ray scattering (SAXS) was performed with a rotating anode generator (Bruker Nanostar, turbospeed solution) equipped with a pinhole camera, and using monochromatized CuKα (λ = 0.154 nm) radiation collimated with crossed Goebel mirrors. The SAXS profiles for the **MOP-Ad** networks were collected in the q range from 0.3 nm^{-1} to 3.5 nm^{-1}. The nitrogen adsorption–desorption isotherms were measured on 3H-2000PM2 analyzer and the adsorption of hydrogen, methane and carbon dioxide analyses was measured on 3H-2000PS2 apparatus at 77 K/1 bar (H_2) and 273 K/1 bar (CH_4 and CO_2). Thermogravimetric analysis (TGA) was performed using a NETZSCH STA 409 PC thermal gravimetric analyzer at a heating rate of 10 °C min^{-1} in nitrogen. SEM analysis was performed on a Hitachi S-3400N scanning electron microscope to investigate the surface morphologies of the polymers. Elemental analysis was performed with a Perkin Elmer Series II 2400 elemental analyzer. All the samples were dried at 200 °C for 24 h under vacuum prior to measurement.

3. Results and discussion

Three **MOP-Ad** networks were synthesized *via* Suzuki coupling polymerization, using TPBA as a so-called "knots" to connect benzene-1,4-diboronic acid, 4,4″-dibromo-*p*-terphenyl, or *p*-terphenyl-4,4″-diboronic acid (TPDBA) "rods", resulting in **MOP-Ad-1**, **MOP-Ad-2** and **MOP-Ad-3**, respectively, as summarized in Scheme 1. The moderate yield of **MOP-Ad-3** (65.7%) was due to the fact that TPDBA was practically a suspension (insoluble) in solvents because of its "long" rod length and thus its participation in the reaction is somewhat limited in contrast to the synthesis of **MOP-Ad-1** (97.7%) and **MOP-Ad-2** (90.2%). Nevertheless, this synthetic approach provides relatively simple, targeted structural diversity and selectivity, as compared with Friedel–Crafts coupling,[17] with moderate to high yield.

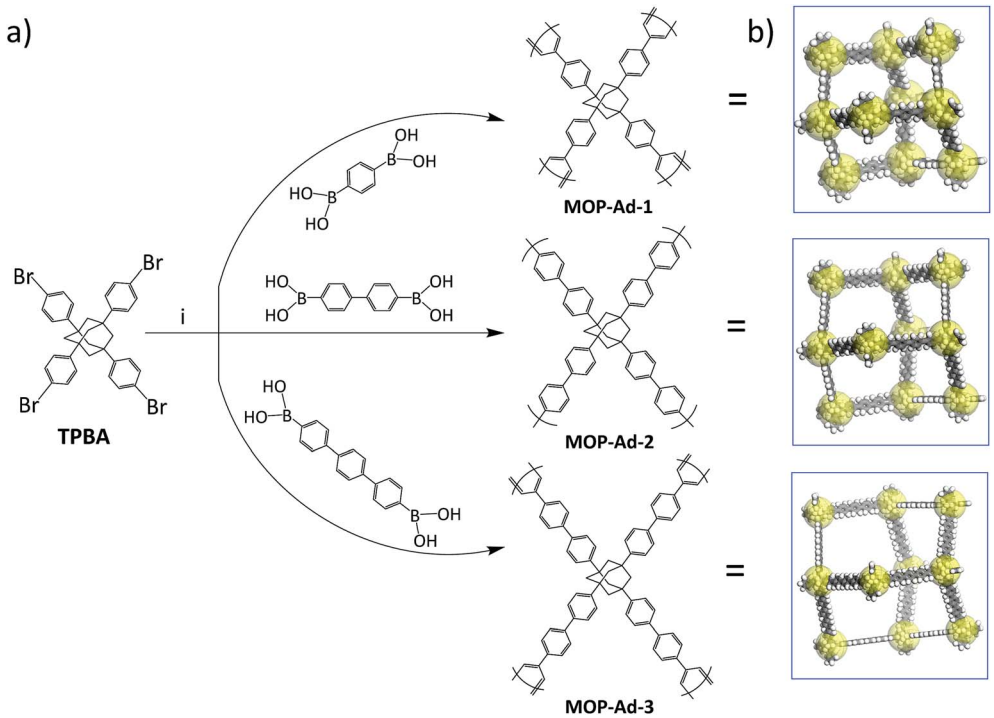

Scheme 1 (a) Synthetic routes to the **MOP-Ad** networks and the notional idealized polymer structures with (b) cartoon 3D representations of the networks in each case.

3.1 Characterization of MOP-Ad networks

FTIR spectroscopy has been widely used in probing the structure of microporous organic polymers. Fig. 1 shows the FTIR spectra of **TBPA** and the corresponding three **MOP-Ad** networks, after subtraction of the KBr background. When comparing the building molecule **TBPA** with its resulting polymers, one of the biggest differences in the spectra is the disappearance of the band at 1070 cm^{-1}, which arises from the C–Br oscillation.[24,25] Furthermore, new bands appeared near 3020 and 1600 cm^{-1} after the coupling polymerization, which are ascribed to the characteristic adsorption of the conjugated system of biphenyl groups.[9,25] The band that appeared at 3430 cm^{-1} is characteristic of the B–OH end-group vibrations in **MOP-Ad** samples[25] and was higher for **MOP-Ad-3**, indicative of a higher number of unreacted termini within the network. Overall, the spectral assignments indicate that the designed MOP networks were successfully synthesized, which is further corroborated by nuclear magnetic resonance (NMR) results (Fig. 2).

^{13}C cross-polarization magic-angle spinning (CP/MAS) NMR spectra with resonance assignment for **MOP-Ad** networks are shown in Fig. 2. There are five main pronounced peaks. For **MOP-Ad-1**, the single peaks at 146.1, 137.1 and 124.6 ppm correspond to the substituted phenyl carbons (C3 at 146.1 ppm

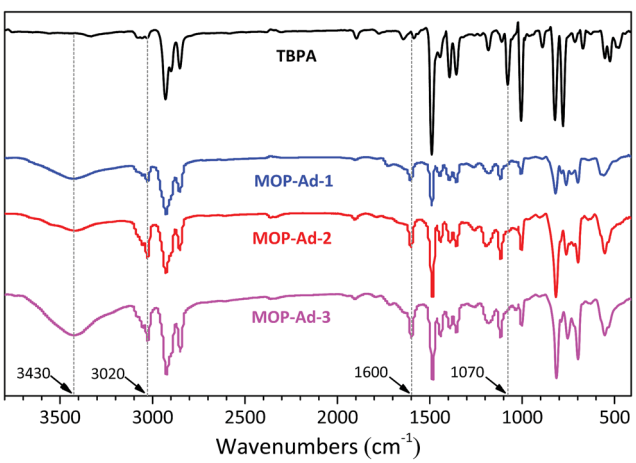

Fig. 1 FTIR spectra for **TBPA** and target polymers, **MOP-Ad-1**, **MOP-Ad-2** and **MOP-Ad-3**.

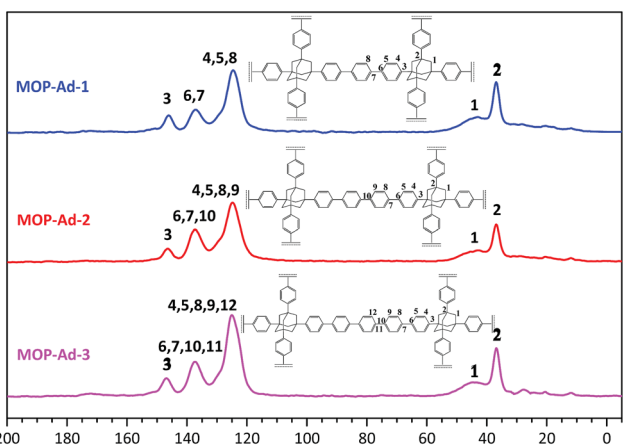

Fig. 2 ^{13}C CP/MAS NMR spectra of **MOP-Ad-1**, **MOP-Ad-2** and **MOP-Ad-3**.

and C6 & C7 at 137.1 ppm) and unsubstituted phenyl carbons (C4, C5 & C8 at 124.6 ppm). Additionally, peaks at 43.0 and 36.7 ppm correspond to the methylene (C1) and quaternary bridgehead carbon (C2) from adamantane, respectively. For **MOP-Ad-2** and **MOP-Ad-3**, all of these peaks can also be observed in the corresponding spectra in Fig. 2. In addition, no clear, sharp diffraction peaks could be observed in the XRD profiles (see ESI Fig. S2†), indicating that the **MOP-Ad** networks are amorphous in nature.

3.2 Stability and porosity of MOP-Ad networks

In comparison with most tetrahedral benzene-based microporous organic polymers, such as those from biphenyl monomer PPN-10 (ref. 26) (stable up to 240 °C), HPOP-2 (ref. 15) (stable up to 280 °C) and triptycene-based STP-4 (ref. 14) (stable up to 300 °C), the three **MOP-Ad** networks in our work do not show a dramatic weight-loss until up to 520 °C (Fig. 3), and exhibit decomposition temperatures over 600 °C. Clearly, the introduction of the rigid adamantane unit has enhanced the thermal stability of our target polymers.[19,22] Moreover, the higher the adamantane content, the better the thermal stability. For example, the molar ratio of adamantane between **MOP-Ad-1** and **MOP-Ad-3** is 22.45% and 14.80%, and we found that **MOP-Ad-1** was more stable (up to 520 °C) than **MOP-Ad-3** (up to 480 °C). This excellent thermal stability is a consequence of the presence of exclusively C–C bonds in the skeletal structure of **MOP-Ad** networks.

To further investigate the stability of **MOP-Ad** networks, the three materials were rigorously stirred at 1500 rpm in hydrochloric acid (2.0 M) and then sodium hydroxide (2.0 M), both for 72 h. Following such harsh treatments, the FTIR spectra (see ESI, Fig. S3†) showed similar bands to the untreated polymers (Fig. 1), demonstrating that **MOP-Ad** materials are structurally stable both in strong acid and base. Similar results were also obtained in the ^{13}C CP/MAS NMR spectra (see ESI Fig. S4†) of the **MOP-Ad** networks before and after acid/base treatment. Moreover, these **MOP-Ad** networks, like many other MOP materials,[18,24] also exhibited excellent chemical stability to common organic solvents such as methanol, acetone, tetrahydrofuran and chloroform.

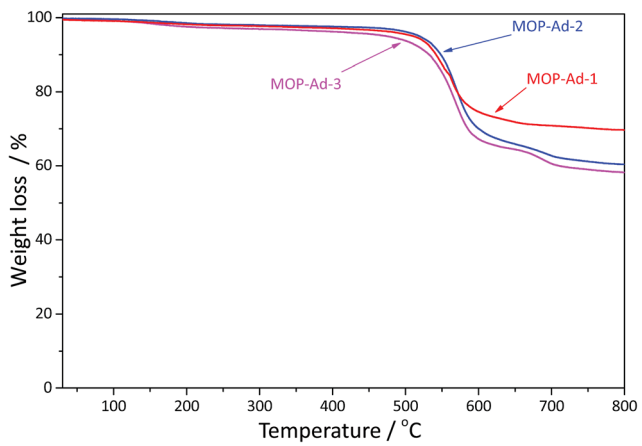

Fig. 3 TGA curves of MOP-Ad-1, MOP-Ad-2 and MOP-Ad-3.

Gas physisorption measurements were conducted to examine the porous nature of the **MOP-Ad** networks. Fig. 4 shows the N_2 adsorption/desorption isotherms and the pore-size distributions (PSD) of the **MOP-Ad** networks, and Table 1 summarizes the porous properties of these polymers at 77.3 K and 1.13 bar. All of the polymers gave rise to type II isotherms (Fig. 4(a)) according to the IUPAC classification.[15] The isotherms clearly displayed a sharp uptake at low relative pressure ($p/p_0 < 0.001$), especially for **MOP-Ad-1** and **MOP-Ad-2**, indicating substantial microporous structure in these networks.[16,27] The upward deviation at higher p/p_0 values for all three **MOP-Ad** networks was also observed, indicating the presence of mesopores in these networks, due to inter-grain porosity or voids.[28] All of the desorption isotherms for the three polymers exhibited hysteresis to some extent, also indicating that these three polymers possess micro- and mesoporous structures. Interestingly, the hysteresis could also indicate a swelling of the polymer matrix or the limited release of trapped nitrogen molecules from the narrow pore channels, which is particularly prevalent for non-ordered nanoporous materials, as described elsewhere.[7,29]

Fig. 4(b) shows the PSD curves for the three **MOP-Ad** networks as calculated using non-local density functional theory (NLDFT).[21] *p*-Terphenyl-4,4″-diboronic acid possesses a larger aspect ratio than both benzene-1,4-diboronic acid and biphenyl-4,4′-diboronic acid. Therefore, after cross-linking, it is logical to anticipate that the longer rod in **MOP-Ad-3** would generate larger pores compared with **MOP-Ad-2** and **MOP-Ad-1**. However, according to Fig. 4(b), the pore diameter of **MOP-Ad-2** and **MOP-Ad-3** appeared at approximately 0.55 nm, and much lower than that of **MOP-Ad-1** (0.74 nm). In particular, with an increased degree of conformational freedom in the longer rod, greater intermolecular and intramolecular intercalation can be obtained in the process of polymerizing, as well as more efficient space filling in the structure.[28,30] Actually, **MOP-Ad-3** possessed a distributed pore diameter ranging from 0.49 to 1.91, owing to the intermolecular and intramolecular intercalation in the network, with SAXS (see ESI Fig. S5†) displaying a less ordered network overall. Field-emission scanning electron microscopy (FE-SEM) (see ESI Fig. S6†) was used to observe the surface morphology of the **MOP-Ad** networks, showing that **MOP-Ad-3** has a certain degree of intercalation while **MOP-Ad-1** and **MOP-Ad-2** exhibit typical agglomerating surfaces.[2,25]

Concomitantly, the surface areas of the **MOP-Ad** networks were shown to be dependent on the length of the rods. Thus, by using different length rods, the BET surface area can be tuned. In the present study, the ranking of the length of rods from the largest to the smallest is *p*-terphenyl-4,4″-diboronic acid, 4,4″-dibromo-*p*-terphenyl and benzene-1,4-diboronic acid. Consequently, the shortest rods between the adamantane rings (**MOP-Ad-1**) exhibited the highest surface areas of 974 $m^2\ g^{-1}$, followed by **MOP-Ad-2** (653 $m^2\ g^{-1}$) and **MOP-Ad-3** (282 $m^2\ g^{-1}$). The same trend in surface area for materials of similar kind was found by Lim *et al.*[17] However, compared with their material (adamantane-3), synthesized from 1-bromoadamantane with terphenyl, *via* Friedel–Crafts reaction, our **MOP-Ad-1** network exhibited a higher BET surface area (974 $m^2\ g^{-1}$ against 720 $m^2\ g^{-1}$). Presumably, this was attributed to the Suzuki coupling

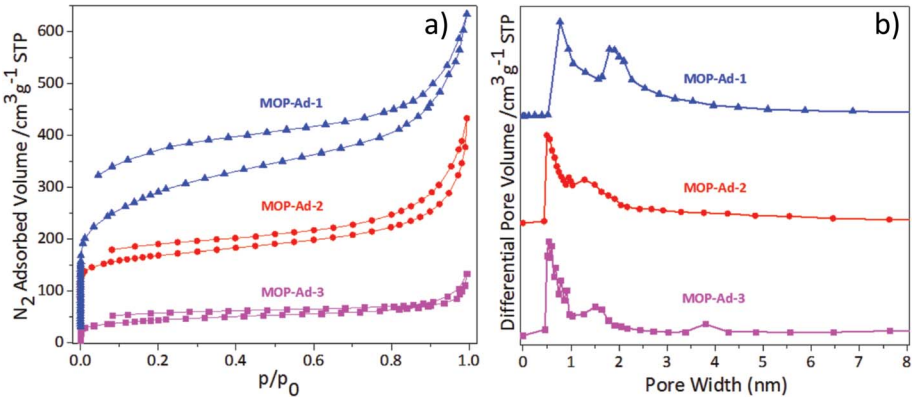

Fig. 4 (a) Nitrogen sorption isotherms of **MOP-Ad-1**, **2** and **3** at 77.3 K and (b) pore size distribution (PSD) for **MOP-Ad-1**, **2** and **3**.

Table 1 Porosity properties and gas uptake capacities of **MOP-Ad** networks

Samples	S_{BET} ($m^2\ g^{-1}$)	V_{micro} [a] ($cm^3\ g^{-1}$)	V_{total} [b] ($cm^3\ g^{-1}$)	V_{micro}/V_{total}	Pore size (nm)
MOP-Ad-1	974	0.27	0.51	0.53	0.74
MOP-Ad-2	653	0.10	0.23	0.43	0.55
MOP-Ad-3	282	0.07	0.11	0.64	0.52

[a] Micropore volume derived from the *t*-plot method. [b] Total pore volume at $p/p_0 = 0.99$.

strategy processing higher selectivity and target activity in the terminal groups (–Br in the knots and $-B(OH)_2$ in the rods) than the Friedel–Crafts reaction (–Br in 1-bromoadamantane and a large number of –H in terphenyl), resulting a large amount of side reactions occurring in the Friedel–Crafts reactions (the possible mechanisms were shown in Scheme S3†).[31–33]

3.3 Gas uptake capabilities

The gas (H_2, CO_2 and CH_4) adsorption performance of all **MOP-Ad** networks were studied to evaluate their applicability in gas storage/purification. In accordance with the results obtained from gas physisorption (Fig. 5 and Table 2) with pressure up to 1.13 bar, one can see that **MOP-Ad-1**, **MOP-Ad-2** and **MOP-Ad-3** exhibited moderate uptake capacities for H_2 (1.07, 0.92 and 0.49 wt%) and CO_2 (10.3, 7.5 and 5.2 wt%), respectively. This gas adsorption performance is comparable to currently favorable microporous organic polymers under the same condition, such as networks based on spirocyclic tetraether (SPOP-8, 0.67 wt% for H_2, 4.2 wt% for CO_2),[34] and triptycene (STP-3 and STP-4, 0.5 and 0.9 wt% for H_2, 6.2 and 7.5 wt% for CO_2, respectively).[14] Nevertheless, the **MOP-Ad** networks were not as effective as PBI-Ad-1 and PBI-Ad-2 (1.6 and 1.3 wt% for H_2, 17.3 and 13.7 wt% for CO_2), which connected 1,3,5,7-tetrakis(4-formylphenyl) adamantane with 3,3′-diaminobenzidine or 1,2,4,5-tetraaminobenzene, respectively.[35] In addition, the physisorption isotherms had not reached saturation state at pressure 1.13 bar for both H_2 and CO_2 uptakes by **MOP-Ad** networks, implying that higher capacities can be expected at increased pressures. Moreover, the H_2 and CO_2 uptake properties of the **MOP-Ad** networks can be directly correlated with the surface area and microporous volume. As expected, the polymers with the highest surface areas and microporous volumes gave rise to the highest H_2 and CO_2 uptakes under the same testing conditions.

CH_4 adsorption of the **MOP-Ad** networks was also investigated; **MOP-Ad-1**, **MOP-Ad-2** and **MOP-Ad-3** (Table 2 and ESI Fig. S7†) exhibited better CH_4 uptake capacities (2.4, 1.6 and 1.0 wt%, respectively) than most non-functionalized porous polymer networks, such as tetrahedral porous frameworks based on 2,2′,7,7′-tetraethynyl-9,9′-spirobifluorene POP-1

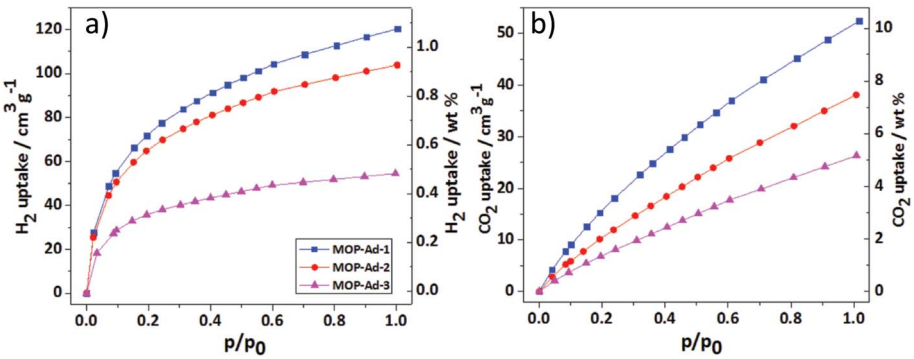

Fig. 5 Gas sorption isotherms (a) H_2 at 77.3 K, (b) CO_2 at 273.1 K.

Table 2 Porosity properties and gas uptake capacities of MOP-Ad networks

Samples	H_2 uptake[a] (wt%)	CO_2 uptake[b] (wt%)	CH_4 uptake[b] (wt%)	Selectivity[c] CO_2/CH_4
MOP-Ad-1	1.07	10.3	2.4	3.8
MOP-Ad-2	0.92	7.5	1.6	5.3
MOP-Ad-3	0.49	5.2	1.0	5.9

[a] Data were obtained at 1.13 bar and 77.3 K. [b] 1.13 bar and 273.1 K. [c] Adsorption selectivity based on the Henry's law.

(0.8 wt%),[2] nanoporous covalent triazine-based frameworks with adamantane PCTF-2 (1.0 wt%),[36] but lower than the fluorinated porous poly(arylene-ethynylenes) FPOP-1 and FPOP-2 (2.7 and 3.3 wt%, respectively)[37] due to the fluorine heteroatoms that enhance interactions between the pore walls and CH_4 molecules.[21]

For CO_2 capture and separation applications, high selectivity is also essential. We estimated the selectivity of CO_2 over CH_4 (*i.e.*, CO_2/CH_4 selectivity) for **MOP-Ad-1**, **MOP-Ad-2** and **MOP-Ad-3** networks by applying Henry's law to the adsorption data at 273.1 K and low pressure (less than 0.15 bar),[16,38] which is typical partial pressure of CO_2 in flue gas. As shown in Table 2, the CO_2/CH_4 selectivities of **MOP-Ad** networks are calculated to be 3.8, 5.3, and 5.9, respectively (see ESI Fig. S8†).

For the adsorption and selectivity performance of **MOP-Ad** networks, **MOP-Ad-1** possesses relatively higher CO_2 and CH_4 uptakes, but **MOP-Ad-3** possesses higher CO_2/CH_4 selectivities. The higher CO_2 and CH_4 uptake is attributed to the higher surface areas and microporous volumes (Table 1). Additional, the narrow pore size distribution also leads to fine selectivity.[39] Although **MOP-Ad-1** showed the highest CO_2 uptake, lower selectivity was obtained due to a higher content of mesoporous surface area and wider pore size distribution in the structure, which apperas to be disadvantageous for the recognition of small CO_2 molecules (3.30 Å) over the large CH_4 (3.82 Å) molecule. Additionally, it was found that the three **MOP-Ad** networks exhibited a slightly lower CO_2/CH_4 selectivity than some functionalized 3D microporous organic polymers, such as tetraphenylethylene-based microporous organic polymers (MTPOPs, 5.4–7.2 at 273 K),[9] and tetraphenyladamantane-based microporous polybenzimidazoles (PBI-Ads, 9.0–11.0 at 273 K),[35] N-doped porous carbons (NAHA, 7.9–10.7 at 273 K),[40] benzothiazole- and benzoxazole-linked porous polymers (6.9–9.4 at 273 K),[38] and the mesoporous polymeric organic frameworks (mesoPOF, 10–15 at 273 K).[41] Again, this difference was attributed to the presence of polarized sites or the utilization of N-rich or O-rich building blocks, which can increase the gas–framework interactions *via* hydrogen bonding or dipole–quadrupole interactions.[42] Care must be taken with such strategies, however, as the introduction of heteroatoms (such as N or O) into networks, as previously reported,[12] reduces the thermal stability of the structure, thus limiting their application. Nevertheless, the CO_2/CH_4 selectivity of the **MOP-Ad** networks was still superior to many other 2D functional polymers, such as carbazole–spacer–carbazole type conjugate microporous networks (3.0–4.0 at 273 K),[43] conjugated microporous copolymers based on 1,3,6,8-tetrabromocarbazole CP-CMP (3.4–4.2 at 273 K),[44] even some 3D functional polymers, such as N-functionalized microporous organic polymer based on tetraethynyl monomer TEPS-TPA (3.9 at 273 K),[45] tetraethynylspirobifluorene-containing porous organic polymers (POP, 3.4–4.8 at 298 K),[2] the tetra-armed triphenylamine-containing MOPs (3.4–4.3 at 273 K),[46] tetrakis(4-ethynylphenyl)methane-based porous materials (PAF-26-COOH, 4.0 at 298 K).[21] Additionally, the adsorption and selectivity performance of **MOP-Ad** networks after immersing in hydrochloric acid and sodium hydroxide were also investigated in the same conditions. As expected, we found no significant changes in the CO_2 and CH_4 uptake capacities (see ESI Fig. S9 and Table S1†), as well as the CO_2/CH_4 selectivities, which reflects their high chemical stability.

4. Conclusions

In summary, three microporous organic polymers (**MOP-Ad**) have been synthesized by Suzuki coupling and a rich structural diversity of them was achieved by using tetraphenyl adamantane "knots" and different phenylboronic acid "rods" as modular building blocks. Importantly, owing to the rational design of the molecular skeleton, these **MOP-Ad** networks not only exhibited extremely high thermal stability (stable up to 520 °C), but were also stable in common organic solvents, and strong acid and base. For potential use as gas storage materials, they showed desirable adsorption ability over small gas molecules. For example, **MOP-Ad-1**, the network with the shortest rod linkers, can reversibly absorb 1.07 wt% H_2 (77.3 K and 1.13 bar), 10.3 wt% CO_2 and 2.4 wt% CH_4 (273.1 K and 1.13 bar). Moreover, the three porous networks showed good CO_2/CH_4 selectivity without any post modification, highlighting them as promising candidates for post-combustion CO_2 capture and separation.

Acknowledgements

This work was supported by National Natural Science Foundation of China (No. 21476051), Science and Technology Program of Guangdong Province (No. 2016A050502057) and Natural Science Foundation of Guangdong Province (No. 2016A030310349). H. Yue is grateful to China Postdoctoral Science Foundation. PDT thanks the State Administration for Foreign Experts Affairs and the Royal Society of Chemistry for a Visiting Researcher Programme grant to China.

References

1 B. Coasne, A. Galarneau, R. J. M. Pellenq and F. D. Renzo, *Chem. Soc. Rev.*, 2013, **42**, 4141–4171.
2 Q. Y. Ma, B. X. Yang and J. Q. Li, *RSC Adv.*, 2015, **5**, 64163–64169.
3 B. Wang, A. P. Côté, H. Furukawa, M. O'keeffe and O. M. Yaghi, *Nature*, 2008, **453**, 207–211.
4 Z. Xiang and D. Cao, *J. Mater. Chem. A.*, 2013, **1**, 2691–2718.
5 S. Xu, Y. Luo and B. Tan, *Macromol. Rapid Commun.*, 2013, **34**, 471–484.

6 T. M. McDonald, W. R. Lee, J. A. Mason, B. M. Wiers, C. S. Hong and J. R. Long, *J. Am. Chem. Soc.*, 2012, **134**, 7056–7065.
7 S. Y. Ding and W. Wang, *Chem. Soc. Rev.*, 2013, **42**, 548–568.
8 H. Furukawa and O. M. Yaghi, *J. Am. Chem. Soc.*, 2009, **131**, 8875–8883.
9 H. Li, X. Ding and B. H. Han, *RSC Adv.*, 2016, **6**, 51411–51418.
10 R. Q. Zhong, Z. L. Xu, W. Z. Bi, S. B. Han, X. F. Yu and R. Q. Zou, *Inorg. Chim. Acta*, 2016, **443**, 299–303.
11 K. V. Rao, R. Haldar, T. K. Maji and S. J. George, *Polymer*, 2014, **55**, 1452–1458.
12 G. Li, B. Zhang, J. Yan and Z. Wang, *J. Mater. Chem. A.*, 2014, **2**, 18881–18888.
13 C. Klumpen, M. Breunig, T. Homburg, N. Stock and J. Senker, *Chem. Mater.*, 2016, **28**, 5461–5470.
14 C. Zhang, Z. Wang, J. J. Wang, L. Tan, J. M. Liu, B. Tan, X. L. Yang and H. B. Xu, *Polymer*, 2013, **54**, 6942–6946.
15 Q. Chen, M. Luo, T. Wang, J. X. Wang, D. Zhou, Y. Han, C. S. Zhang, C. G. Yan and B. H. Han, *Macromolecules*, 2011, **44**, 5573–5577.
16 C. Zhang, X. Yang, Y. Zhao, X. Wang, M. Yu and J. X. Jiang, *Polymer*, 2015, **61**, 36–41.
17 H. Lim, M. C. Cha and J. Y. Chang, *Polym. Chem.*, 2012, **3**, 868–870.
18 H. Lim and J. Y. Chang, *Macromolecules*, 2010, **43**, 6943–6945.
19 S. Q. Fu, J. W. Guo, D. Y. Zhu, Z. Yang, C. F. Yang, J. X. Xian and X. Li, *RSC Adv.*, 2015, **5**, 67054–67065.
20 R. K. Totten, M. H. Weston, J. K. Park, O. K. Farha, J. T. Hupp and S. T. Nguyen, *ACS Catal.*, 2013, **3**, 1454–1459.
21 H. Ma, H. Ren, X. Zou, S. Meng, F. Sun and G. Zhu, *Polym. Chem.*, 2014, **5**, 144–152.
22 J. W. Guo, X. F. Lai, S. Q. Fu, H. B. Yue, J. W. Wang and P. D. Topham, *Mater. Lett.*, 2017, **187**, 76–79.
23 B. J. Dahl and N. S. Mills, *Org. Lett.*, 2008, **10**, 5605–5608.
24 W. Lu, D. Yuan, D. Zhao, C. I. Schilling, O. Plietzsch, T. Muller, S. Bräse, J. Guenther, J. Blümel, R. Krishna, Z. Li and H. C. Zhou, *Chem. Mater.*, 2010, **22**, 5964–5972.
25 Y. Yuan, F. Sun, H. Ren, X. Jing, W. Wang, H. Ma, H. Zhao and G. Zhu, *J. Mater. Chem.*, 2011, **21**, 13498–13502.
26 W. Lu, Z. Wei, D. Yuan, J. Tian, S. Fordham and H. C. Zhou, *Chem. Mater.*, 2014, **26**, 4589–4597.
27 K. S. W. Sing, D. H. Everett, R. A. W. Haul, L. Moscou, R. A. Pierotti, J. Rouquérol and T. Siemieniewska, *Pure Appl. Chem.*, 1985, **57**, 603–619.
28 J. X. Jiang, F. Su, A. Trewin, C. D. Wood, H. Niu, J. T. A. Jones, Y. Z. Khimyak and A. I. Cooper, *J. Am. Chem. Soc.*, 2008, **130**, 7710–7720.
29 J. Weber, J. Schmidt, A. Thomas and W. Böhlmann, *Langmuir*, 2010, **26**, 15650–15656.
30 J. X. Jiang, A. Trewin, F. Su, C. D. Wood, H. Niu, J. T. A. Jones, Y. Z. Khimyak and A. I. Cooper, *Macromolecules*, 2009, **42**, 2658–2666.
31 Z. Tian, J. Huang, Z. Zhang, G. Shao, A. Liu and S. Yuan, *Microporous Mesoporous Mater.*, 2016, **234**, 130–136.
32 Y. Yang, Q. Zhang, S. Zhang and S. Li, *Polymer*, 2013, **54**, 5698–5702.
33 J. H. Zhu, Q. Chen, Z. Y. Sui and B. H. Han, *J. Mater. Chem. A.*, 2014, **2**, 16181–16189.
34 M. Y. Jiang, Q. Wang, Q. Chen, X. M. Hu, X. L. Ren, Z. H. Li and B. H. Han, *Polymer*, 2013, **54**, 2952–2957.
35 B. Zhang, G. Li, J. Yan and Z. Wang, *J. Phys. Chem. C*, 2015, **119**, 13080–13087.
36 A. Bhunia, I. Boldog, A. Möller and C. Janiak, *J. Mater. Chem. A.*, 2013, **1**, 14990–14999.
37 D. P. Liu, Q. Chen, Y. C. Zhao, L. M. Zhang, A. D. Qi and B. H. Han, *ACS Macro Lett.*, 2013, **2**, 522–526.
38 M. G. Rabbani, T. Islamoglu and H. M. El-Kaderi, *J. Mater. Chem. A.*, 2017, **5**, 258–265.
39 K. Y. Yuan, C. Liu, J. H. Han, G. P. Yu, J. Y. Wang, H. M. Duan, Z. G. Wang and X. G. Jian, *RSC Adv.*, 2016, **6**, 12009–12020.
40 B. Yuan, J. Wang, Y. X. Chen, X. F. Wu, H. M. Luo and S. G. Deng, *J. Mater. Chem. A.*, 2016, **4**, 2263–2276.
41 A. P. Katsoulidis and M. G. Kanatzidis, *Chem. Mater.*, 2012, **24**, 471–479.
42 Q. Chen, M. Luo, P. Hammershøj, D. Zhou, Y. Han, B. W. Laursen, C. G. Yan and B. H. Han, *J. Am. Chem. Soc.*, 2012, **134**, 6084–6087.
43 S. Qiao, Z. Du and R. Yang, *J. Mater. Chem. A.*, 2014, **2**, 1877–1885.
44 M. Yu, X. Wang, X. Yang, Y. Zhao and J. X. Jiang, *Polym. Chem.*, 2015, **6**, 3217–3223.
45 H. J. Zhang, C. Zhang, X. C. Wang, Z. X. Ze, X. M. Liang, B. Chen, J. W. Xu, J. X. Jiang, Y. D. Li, H. Li and F. Wang, *RSC Adv.*, 2016, **6**, 113826–113833.
46 X. Yang, S. W. Yao, M. Yu and J. X. Jiang, *Macromol. Rapid Commun.*, 2014, **35**, 834–839.

